

光学学报

基于双环光电振荡器的频分复用光纤光栅传感系统

高玲歌, 汪弋平*, 田孝忠, 朱丹, 肖云浩, 葛嘉炜, 陈莹莹

南京师范大学计算机与电子信息学院, 江苏省光电技术重点实验室, 江苏 南京 210023

摘要 提出了一种基于双环光电振荡器(OEO)的频分复用光纤布拉格光栅(FBG)传感系统。在该传感系统中,从两个级联的FBG反射的光信号经马赫-曾德尔调制器调制后进入光路的双环结构,两路光信号经耦合后再通过波分复用分成两路,由光电探测器还原为电信号。该电信号分别通过两个不同中心频率的电带通滤波器后形成稳定的微波振荡,输出两路微波信号,分别对应两个FBG传感器。最后,通过对两路微波信号的频率漂移进行测量,最终实现传感解调。实验中对两个FBG分别施加应变和温度,结果表明:传感系统的应变灵敏度为 $0.100\text{ kHz}/\mu\epsilon$,最大频率偏移 0.035 kHz ,对应 $0.35\ \mu\epsilon$ 的测量误差;温度灵敏度为 $1.135\text{ kHz}/^\circ\text{C}$,最大频率偏移 0.072 kHz ,对应 $0.06\ ^\circ\text{C}$ 的测量误差。该系统借助双环OEO的结构,具有稳定性高、测量误差小的优点。

关键词 传感器; 光电振荡器; 微波光子学; 频分复用; 光纤光栅

中图分类号 TN29

文献标志码 A

DOI: 10.3788/AOS230700

1 引言

光纤布拉格光栅(FBG)传感器由于其重量轻、体积小、灵敏度高、抗电磁干扰、在恶劣环境中稳定性好等独特优势被广泛研究^[1]。FBG传感器是一种波长编码的光纤传感器,因此,对FBG谐振波长变化的精确测量是实现高精度传感的关键。目前,传统的FBG传感解调方法如边缘滤波法、扫描激光法、光栅匹配法、CCD光谱法和可调谐F-P滤波器解调法等^[2-3]大多数是在光域内进行的。然而,边缘滤波法测量精度不高,多点同时测量困难;扫描激光法检测速度偏慢,系统成本高且测量范围小;而CCD光谱法检测速度较快,多点复用简单,但CCD分辨率较低;可调谐F-P滤波器解调法较为成熟,但受压电陶瓷的蠕动性和迟滞性等非线性特性的影响,波长检测精度依然不高。基于以上不足之处,研究具有高速度和高分辨率的新型解调技术依然具有重要的意义。近年来,随着微波光子学(MWP)的不断发展,基于MWP的光纤传感解调技术成为该领域的热点之一^[4-5]。MWP是一个新型的交叉学科,其将微波工程与光电子学结合起来,研究微波信号与光信号之间的相互作用^[6-7]。受益于成熟的电谱分析技术以及微波和光信号之间的巨大频率差,基于MWP的光纤传感器具有分辨率高、速度快、稳定性好

等优势^[8]。其工作原理是将携带传感信息的光波参量的变化映射到微波域中微波信号的变化,如微波光子链路的频率响应变化^[9]、微波信号的强度变化^[10]和相移变化^[11]等。与光信号相比,微波信号具有相对较低的频率,能够被更快速的检测^[12]。其中,光电振荡器(OEO)^[13-14]能直接产生低相位噪声的高质量微波信号,在FBG的传感解调技术中展现较大的潜力^[15-18]。其解调原理是将待测量引起的光域中的参数(如谐振波长)变化映射到微波域中的振荡频率偏移,从而实现微波领域传感信息的高分辨率和快速处理。然而,目前基于OEO的FBG传感器大多是单环结构,且采用光纤作为储能元件,光纤长度越长,OEO输出微波的频率间隔就越小,只有通过高性能的电带通滤波器(EBPF)才能实现模式选择,从而使OEO稳定地输出主谐振模式信号,实现高精度传感。为了克服以上问题,Tian等^[19]利用游标效应将OEO的自由频谱范围(FSR)从 301.5 kHz 提高到 10.4 MHz ,实现高灵敏度的应变传感。但这种方案只能实现单一待测量的检测。Feng^[20]提出使用两个独立的OEO实现磁场和温度的同时传感,但该系统需要两套OEO设备,其结构复杂且成本高昂,不利于网络化发展。因此,亟需提出一种拥有较强组网能力的、可实现传感网络构建的基于OEO的FBG传感器。

收稿日期: 2023-03-24; 修回日期: 2023-04-29; 录用日期: 2023-05-25; 网络首发日期: 2023-06-05

基金项目: 国家自然科学基金(61975082, 62205149)

通信作者: *jeremy_ff@sina.com

针对以上问题,本文提出了一种基于双环OEO的FBG传感解调方案。传感器中采用了两个级联的FBG分别作为应变和温度的传感头,然后在环路中构建两个长度差很大的光环路1和光环路2,形成光路双环OEO结构,再通过波分复用(WDM)将光信号分成两路,通过两个不同中心频率的EBPF进行频分复用,最后利用波长到频率的映射机制解调出应变和温度。需要指出的是,光环路2由长度约为5 m的可调光衰减器(VOA)及其尾纤构成,该环路用作模式滤波器。因此,传感器的模式选择能力得到增强,降低了不期望模式的增益竞争能力和电放大器(EA)的功耗,大部分增益被主谐振模式占据,减少了跟踪信号的频率波动。最重要的是,该传感器通过频分复用技术实现应变和温度的同时传感,展现出非常明显的组网优势。

2 基本原理

图 1 为基于双环 OEO 的频分复用 FBG 传感器的

结构示意图。该传感器由宽谱光源(ASE)、环形器(CIR)、FBG、马赫-曾德尔调制器(MZM)、掺铒光纤放大器(EDFA)、耦合器(OC)、VOA、色散补偿光纤(DCF)、WDM、光电探测器(PD)、EA、EBPF、电功分器(EC)和电谱分析仪(ESA)组成。ASE输出的光由两个FBG反射后进入MZM调制,调制后的两个光载波通过EDFA,为OEO系统提供足够的光功率。两个光载波通过OC沿着两个不同长度的光路传播。两条光路一个由DCF构成,另一个由VOA及其尾纤构成,VOA的作用是平衡两个光路之间的光功率,从而获得较高的信噪比(SNR)。具有不同延迟的两个光载波在第二个OC处被耦合,再经过WDM被分成两路,两路光载波通过PD最终转换为相应的微波信号,微波信号通过EA放大、EBPF滤波,选出所需的频率。最终,经过滤波的两个微波信号通过EC一部分被发送到ESA进行观察,另一部分被反馈到MZM以形成OEO闭合回路。

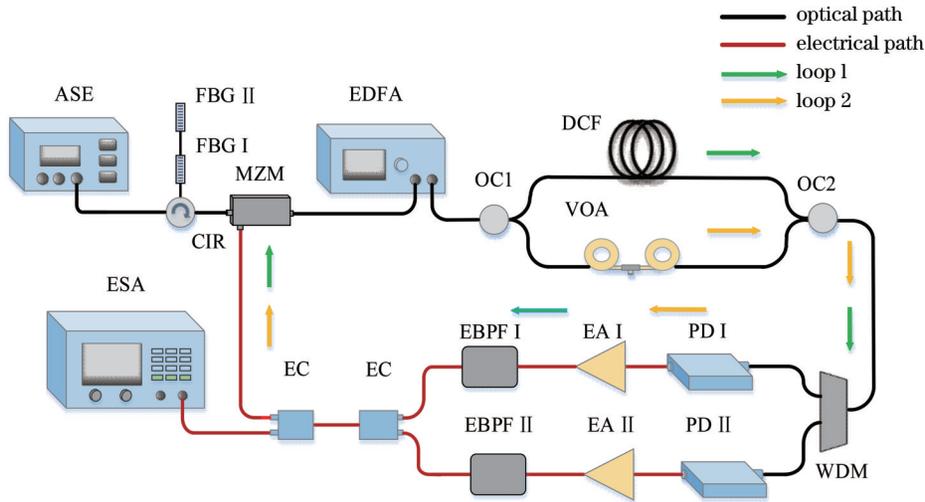


图 1 基于双环 OEO 的频分复用 FBG 传感系统

Fig. 1 Frequency division multiplexing FBG sensing system based on the dual-loop OEO

基于 OEO 的工作原理, OEO 的振荡频率由环路的总时延 τ 决定。 τ 可表示为^[19]

$$\tau_i = \tau_{oi} + \tau_e, \quad i = 1, 2, \quad (1)$$

式中: τ_{oi} 和 τ_e 分别为光路和电路的时延, i 为环路 1 和环路 2。如图 1 所示, 双环 OEO 由两个光路组成, 时延分别为 $\tau_{o1} = (n_{DCF}L_{DCF} + n_{SMF}L_{SMF})/c$ 、 $\tau_{o2} = n_{SMF}L_{SMF}/c$, n_{DCF} 、 n_{SMF} 为 DCF 和单模光纤(SMF)的有效折射率, L_{DCF} 和 L_{SMF} 为 DCF 和 SMF 的长度, c 为真空中的光速。单环 OEO 输出的微波振荡频率 f 和自由光谱范围(FSR) R_{FSi} 可表示为^[19]

$$R_{FSi} = \frac{1}{\tau_i}, \quad (2)$$

$$f_i = N_i \cdot R_{FSi}, \quad (3)$$

式中: N_i 为 OEO 输出的第 N 次谐振模式。当 FBG 上施加应变或温度时, 会引起 FBG 的谐振波长偏移, 借

助 DCF 的色散效应, 谐振波长偏移又会引起 OEO 环路的总时延变化, 从而使 OEO 输出的微波振荡频率偏移, 实现波长到频率的映射。结合式(1)~式(3), 单环 OEO 总时延变化 $\Delta\tau$ 和输出的微波振荡频率偏移量 Δf_i 可表示为

$$\Delta\tau_i = D_i \cdot \Delta\lambda_{FBG} = D_i \cdot \lambda_{FBG} \cdot (K_\epsilon \cdot \epsilon + K_T \cdot \Delta T), \quad (4)$$

$$\Delta f_i = N_i \cdot \Delta R_{FSi} = N_i \cdot \left(\frac{1}{\tau_i + \Delta\tau_i} - \frac{1}{\tau_i} \right) \approx$$

$$-N_i \cdot \frac{\Delta\tau_i}{\tau_i^2} = -f_i \cdot R_{FSi} \cdot \Delta\tau_i, \quad \tau_\Delta \ll \tau, \quad (5)$$

式中: D_i 为环路 1 中的 DCF 和环路 2 中的 SMF 的色散值; λ_{FBG} 为 FBG 的谐振波长; $\Delta\lambda_{FBG}$ 为 FBG 谐振波长偏移量; ϵ 、 T 分别为施加在 FBG 上的应变和温度; K_ϵ 、 K_T 为应变系数和温度系数。由于该传感器中两个光路存在较大的长度差, 短环路 2 可使长环路 1 的 FSR 值加

倍,即只有同时满足两个环路振荡条件的谐振模式才能稳定输出,从而实现了双环OEO输出的微波振荡频率有较大的FSR和低相位噪声,所以双环OEO的FSR主要由短环路2决定,可表示为

$$R_{FS\text{dual}} = R_{FS2}, \quad (6)$$

式中: R_{FS2} 为环路2的FSR。结合式(3),双环OEO输出的微波振荡频率 f_{dual} 可表示为

$$f_{\text{dual}} = N_{\text{dual}} \cdot R_{FS\text{dual}}, \quad (7)$$

式中: N_{dual} 为双环OEO输出的第 N 次谐振模式。

由于环路2中SMF的色散值很小,引起的时延变化 $\Delta\tau$ 可以忽略,所以 $\Delta\lambda_{\text{FBG}}$ 引起的 $\Delta\tau$ 主要发生在环路1的DCF中,即双环OEO输出的微波振荡频率偏移量 Δf_{dual} 由环路1决定。 Δf_{dual} 可表示为

$$\Delta f_{\text{dual}} = \Delta f_1, \quad (8)$$

结合式(4)、式(5)和式(8)可知,两个双环OEO的 Δf_{dual} 可表示为

$$\Delta f_{\text{dual I}} = -f_{\text{dual I}} \cdot R_{FS1} \cdot D_{\text{FBG I}} \cdot \lambda_{\text{FBG I}} \cdot K_{\epsilon} \cdot \epsilon, \quad (9)$$

$$\Delta f_{\text{dual II}} = -f_{\text{dual II}} \cdot R_{FS1} \cdot D_{\text{FBG II}} \cdot \lambda_{\text{FBG II}} \cdot K_T \cdot \Delta T, \quad (10)$$

式中: $D_{\text{FBG I}}$ 、 $D_{\text{FBG II}}$ 为两个FBG波长在DCF上对应的总色散值; $f_{\text{dual I}}$ 、 $f_{\text{dual II}}$ 为两个双环OEO输出的跟踪信号。由式(9)、式(10)可知,OEO输出的 Δf_{dual} 与施加到FBG的待测量 ϵ 和 T 具有良好的线性关系,可以通过同时监测OEO输出的两个微波振荡频率解调出待测量,从而实现传感。同时,提高DCF的色散值 D 和EBPF的中心频率还能获得更高灵敏度的传感器。

3 分析与讨论

实验中,FBG I和FBG II的谐振波长分别为1551.02 nm和1535.03 nm,且两个FBG在DCF上对应的色散值为 -225.73 ps/(nm·km)和 -168.94 ps/(nm·km),DCF总长度约为1129 m,因此,总色散值 $D_{\text{FBG I}}$ 和 $D_{\text{FBG II}}$ 为 -254.85 ps/nm和 -190.73 ps/nm。EBPF I和EBPF II的中心频率分别为1.98976 GHz和3.23254 GHz,3 dB带宽为300 MHz和100 MHz。在光域中测得应变系数 K_{ϵ} 和温度系数 K_T 分别为 $0.78 \times 10^{-5} \mu\epsilon^{-1}$ 和 $7.5 \times 10^{-6} \text{ } ^\circ\text{C}^{-1}$ 。

图2(a)为所提的两个双环OEO传感器初始状态下的响应, $f_{\text{dual I}}$ 和 $f_{\text{dual II}}$ 分别为双环OEO I和双环OEO II经过EBPF滤波后输出的微波振荡信号, f_{beat} 为两个振荡信号的拍频信号, $f_{\text{beat}} = f_{\text{dual II}} - f_{\text{dual I}}$ 。当断开光环路2时,形成两个单环OEO传感器, $f_{\text{single I}}$ 和 $f_{\text{single II}}$ 分别为单环OEO I和单环OEO II输出的微波振荡信号。由于单环OEO输出的振荡信号不稳定,导致拍频信号功率较弱,从而难以形成稳定的振荡模式,所以在此处不给出单环OEO中的拍频信号。图2(b)为 f_{beat} 信号放大图,由图2(b)可知, f_{beat} 约为1.24571 GHz,其FSR约为5.01 MHz,这对应约41 m的环路2长度。主谐振模式和最近的谐振模式之间的边模抑制比

(SMSR)约为18.5 dB。图2(c)为 $f_{\text{dual I}}$ 信号放大图,可以观察到 $f_{\text{dual I}}$ 约为1.98938 GHz,其FSR约为5.01 MHz,SMSR约为23.9 dB。内页为 $f_{\text{single I}}$ 信号放大图,其FSR约为177 kHz,SMSR约为5.9 dB。不难看出,在EBPF I通带内, $f_{\text{single I}}$ 的FSR由177 kHz提高到5.01 MHz,SMSR从5.9 dB增加到23.9 dB。该结果表明:与传统单环OEO传感器相比,所提的双环OEO传感器的FSR约为单环的28倍。由于增益竞争效应,其他模式被有效抑制,只剩下一个主谐振模式捕获OEO中的大部分增益,分配给其他模式的增益始终较弱,从而确保稳定的主谐振模式输出,传感器的模式选择能力明显增强。通过跟踪该主谐振模式,传感性能也会很稳定。与上述类似,图2(d)为 $f_{\text{dual II}}$ 信号放大图, $f_{\text{dual II}}$ 约为3.23509 GHz,其FSR约为5.01 MHz,SMSR约为26.5 dB。图2(d)插图中 $f_{\text{single II}}$ 的FSR和SMSR分别为177 kHz和5.9 dB。

在FBG传感特性的测量中,双环OEO I中FBG I反射的谐振波长经过WDM后由PD I还原为微波振荡信号,再经过EA I放大,最后进入EBPF I滤波。选择频率为1.98938 GHz的主谐振模式作为跟踪信号 $f_{\text{dual I}}$ 测量应变。与上述测量过程类似,双环OEO II中选择频率为3.23509 GHz的主谐振模式作为跟踪信号 $f_{\text{dual II}}$ 测量温度。

首先,以 $45 \mu\epsilon$ 和 $6 \text{ } ^\circ\text{C}$ 为步长,逐步增加FBG上的应变 ϵ 和温度 T ,测量范围分别为 $0 \sim 540 \mu\epsilon$ 和 $24 \sim 96 \text{ } ^\circ\text{C}$ 。 ϵ 和 $\Delta f_{\text{dual I}}$ 呈良好的线性关系如图3(a)、图3(b)所示,且 $f_{\text{dual I}}$ 随着施加到FBG上的 ϵ 增加而向高频范围偏移。拟合结果表明:基于双环OEO的FBG应变传感器的灵敏度约为 $0.100 \text{ kHz}/\mu\epsilon$,这与理论推导的灵敏度 $0.108 \text{ kHz}/\mu\epsilon$ 基本一致, R^2 为0.998。 $\Delta f_{\text{dual II}}$ 随着 T 的增加而向高频范围线性移动如图3(c)、图3(d)所示。基于双环OEO的FBG温度传感器的灵敏度约为 $1.135 \text{ kHz}/\text{ } ^\circ\text{C}$,这与 $1.266 \text{ kHz}/\text{ } ^\circ\text{C}$ 的理论灵敏度大体一致, R^2 为0.998。

其次,为了避免出现频率模糊,传感器的测量范围会受到OEO的FSR限制。在实验中,断开VOA所在的光环路2形成基于单环OEO频分复用的FBG应变、温度传感器。实验测得其FSR为177 kHz,应变灵敏度和温度灵敏度分别为 $0.111 \text{ kHz}/\mu\epsilon$ 和 $1.170 \text{ kHz}/\text{ } ^\circ\text{C}$,因此可测得最大应变和温度为 $1595 \mu\epsilon$ 和 $151 \text{ } ^\circ\text{C}$ 。而所提的基于双环OEO频分复用的FBG应变、温度传感器的FSR为5.01 MHz,传感器的灵敏度为 $0.100 \text{ kHz}/\mu\epsilon$ 和 $1.135 \text{ kHz}/\text{ } ^\circ\text{C}$,通过简单计算可以看出,基于双环OEO的FBG传感器其测量范围远超FBG的最大可承受应变量和温度^[21-22]。因此,与单环结构相比,双环结构能在几乎不影响传感器灵敏度的前提下,大幅提高传感器的测量范围。考虑到传感器的分辨率会受到ESA最小频率分辨率的限制,传感器固定的应变灵敏度为 $0.100 \text{ kHz}/\mu\epsilon$ 和温度灵敏度

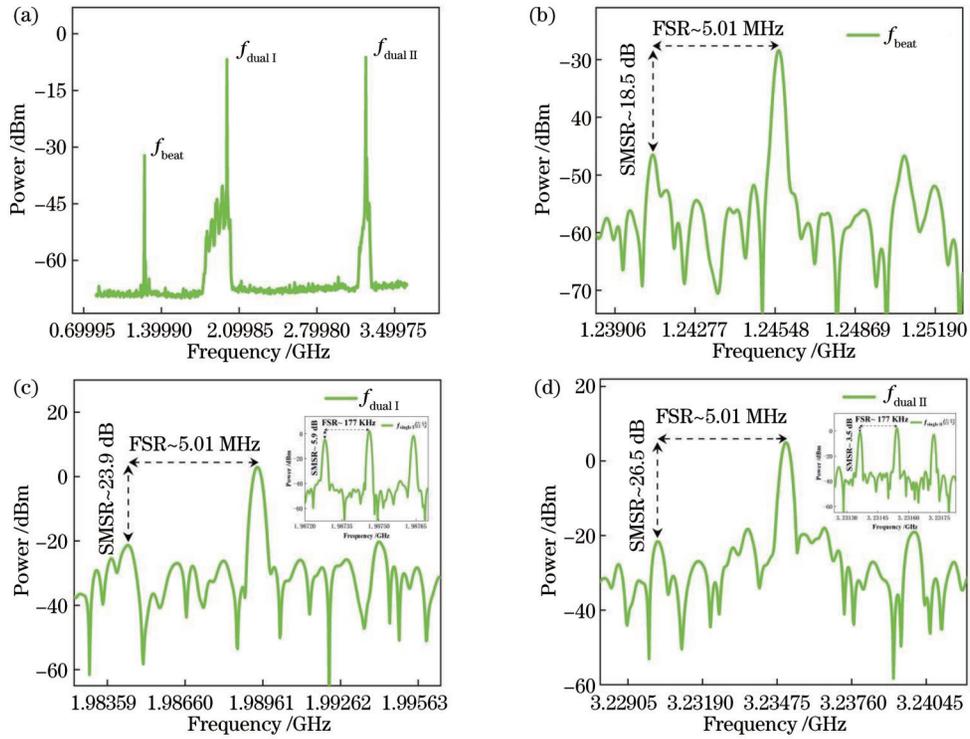


图 2 整体的振荡频率情况。(a) 传感器初始状态下的响应；(b) 振荡频率 f_{beat} ；(c) 振荡频率 $f_{dual I}$ ，插图为振荡频率 $f_{single I}$ ；(d) 振荡频率 $f_{dual II}$ ，插图为振荡频率 $f_{single II}$

Fig. 2 Overall oscillation frequency. (a) Response of the sensor in initial state; (b) oscillation frequency f_{beat} ; (c) oscillation frequency $f_{dual I}$, insert is oscillation frequency $f_{single I}$; (d) oscillation frequency $f_{dual II}$, insert is oscillation frequency $f_{single II}$

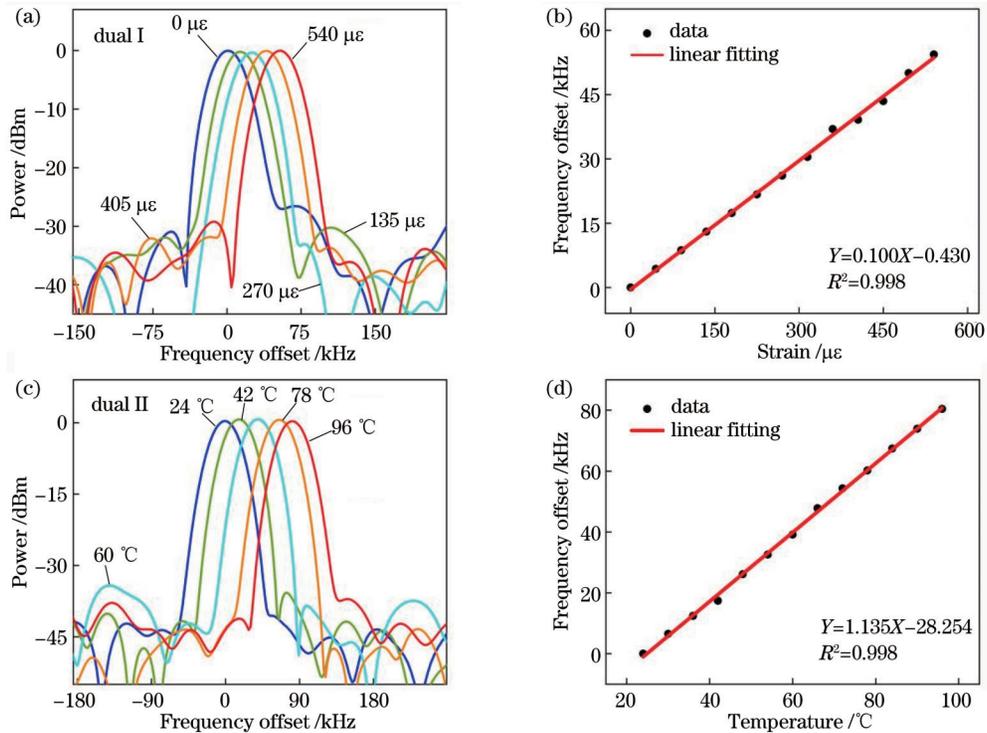


图 3 不同应变和温度下双环 OEO 的响应。(a) 双环 OEO 在不同应变下产生信号的微波谱；(b) 频率和应变变化之间的关系；(c) 双环 OEO 在不同温度下产生信号的微波谱；(d) 频率和温度变化之间的关系

Fig. 3 Response of the dual-loop OEO at different strains and temperatures. (a) Microwave spectrum of the signal generated by dual-loop OEO under different strains; (b) relationship between frequency and strain variation; (c) microwave spectrum of signals generated by dual-loop OEO at different temperatures; (d) relationship between frequency and temperature variation

为 1.135 kHz/°C, 当 ESA 的最小频率分辨率为 1 Hz 时, 传感器的应变分辨率为 $1 \times 10^{-4} \mu\epsilon$, 温度分辨率为 $9 \times 10^{-4} \text{ }^\circ\text{C}$ 。该结果表明: 所提的传感器具有良好的分辨率。

最后, 评估了基于单环 OEO 和基于双环 OEO 的传感器的稳定性。当 FBG I 上的应变分别恒定为 0、270、540 $\mu\epsilon$, FBG II 上的温度分别恒定为 24、60、96 $^\circ\text{C}$ 时, 测试在每个应变和温度下, 10 min 内 OEO 输出的振荡频率偏移量。测量结果如图 4 所示, 图 4(a) 表明

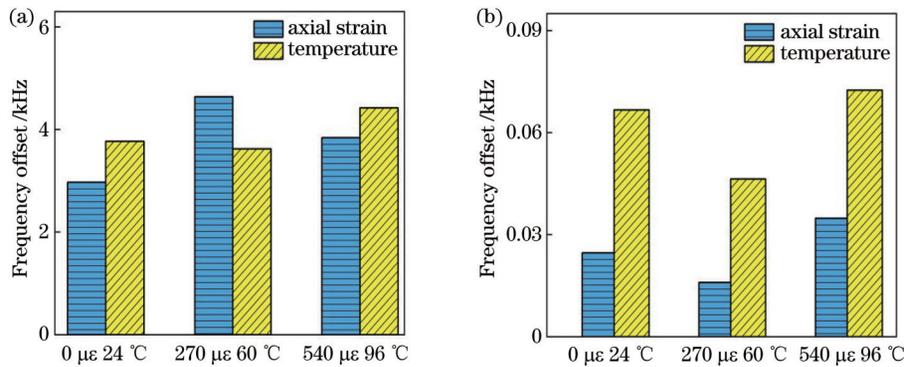


图 4 OEO 振荡频率的稳定性。(a) 单环 OEO 振荡频率的稳定性; (b) 双环 OEO 振荡频率的稳定性

Fig. 4 Stability of OEO oscillation frequency. (a) Stability of the single-loop OEO oscillation frequency; (b) stability of the dual-loop OEO oscillation frequency

4 结 论

提出了一种基于双环 OEO 频分复用的多功能传感器并通过实验验证其性能。配置两个长度相差较大的光路引入双环 OEO 结构, 将 FSR 扩大大约 28 倍, 提高待测量的测量范围。与基于单环 OEO 传感器 42 $\mu\epsilon$ 和 4 $^\circ\text{C}$ 的测量误差相比, 理论上双环 OEO 的测量误差仅为 0.35 $\mu\epsilon$ 和 0.06 $^\circ\text{C}$, 这使得传感器具有高稳定性、大测量范围和小测量误差等优点。通过 WDM 和两个不同中心频率的 EBPF 进行频分复用形成两个双环 OEO 结构, 使得应变和温度可以同时进行传感, 并在实验中得到 0.100 kHz/ $\mu\epsilon$ 和 1.135 kHz/ $^\circ\text{C}$ 的传感灵敏度。此外, 将更密集的 WDM 和更多不同中心频率的 EBPF 应用到所提的传感器中, 就能以组网的形式实现更多待测量的传感。

参 考 文 献

- [1] Kersey A D, Davis M A, Patrick H J, et al. Fiber grating sensors[J]. Journal of Lightwave Technology, 1997, 15(8): 1442-1463.
- [2] 李岚, 董新永, 赵春柳, 等. 强度解调型光纤布拉格光栅传感器的研究及进展[J]. 激光与光电子学进展, 2010, 47(9): 090603.
Li L, Dong X Y, Zhao C L, et al. Research and development of intensity-modulated fiber Bragg grating sensors[J]. Laser & Optoelectronics Progress, 2010, 47(9): 090603.
- [3] 李志全, 许明妍, 汤敬, 等. 光纤光栅传感系统信号解调技术的研究[J]. 应用光学, 2005, 26(4): 36-41, 45.
Li Z Q, Xu M Y, Tang J, et al. Study on techniques of signal demodulation in fiber Bragg grating sensing system[J]. Journal of Applied Optics, 2005, 26(4): 36-41, 45.
- [4] Chen L R, Comanici M I, Moslemi P, et al. A review of recent results on simultaneous interrogation of multiple fiber Bragg grating-based sensors using microwave photonics[J]. Applied Sciences, 2019, 9(2): 298.
- [5] Li L W, Yi X K, Chew S X, et al. Double-pass microwave photonic sensing system based on low-coherence interferometry[J]. Optics Letters, 2019, 44(7): 1662-1665.
- [6] 何刚, 瞿鹏飞, 孙力军. 微波光子技术应用现状及趋势[J]. 半导体光电, 2017, 38(5): 627-632.
He G, Qu P F, Sun L J. Application status and trend of microwave photonic technology[J]. Semiconductor Optoelectronics, 2017, 38(5): 627-632.
- [7] 李明, 郝腾飞, 李伟. 微波光子与多学科交叉融合的前景展望(特邀)[J]. 红外与激光工程, 2021, 50(7): 20211042.
Li M, Hao T F, Li W. Prospects of cross research between microwave photonics and multidiscipline(Invited)[J]. Infrared and Laser Engineering, 2021, 50(7): 20211042.
- [8] Fan Z Q, Su J, Zhang T H, et al. High-precision thermal-insensitive strain sensor based on optoelectronic oscillator[J]. Optics Express, 2017, 25(22): 27037-27050.
- [9] Cheng R, Xia L, Yan J, et al. Radio frequency FBG-based interferometer for remote adaptive strain monitoring[J]. IEEE Photonics Technology Letters, 2015, 27(15): 1577-1580.
- [10] Zhou J A, Xia L, Cheng R, et al. Radio-frequency unbalanced M-Z interferometer for wavelength interrogation of fiber Bragg grating sensors[J]. Optics Letters, 2016, 41(2): 313-316.
- [11] Wang J, Zhu W S, Ma C Y, et al. FBG wavelength demodulation based on a radio frequency optical true time delay method[J]. Optics Letters, 2018, 43(11): 2664-2667.
- [12] 崔益峰, 汪弋平, 施青云, 等. 基于微波光子滤波器的高分辨率光纤横向负载传感器[J]. 光学学报, 2018, 38(12): 1206004.
Cui Y F, Wang Y P, Shi Q Y, et al. High-resolution transverse load fiber sensor based on microwave photonic filter[J]. Acta Optica Sinica, 2018, 38(12): 1206004.

- [13] 梁建惠, 江阳, 白光富, 等. 光路往返的双环路光电振荡器[J]. 光学学报, 2014, 34(4): 0406002.
Liang J H, Jiang Y, Bai G F, et al. Dual-loop optoelectronic oscillator with reciprocating optical path[J]. Acta Optica Sinica, 2014, 34(4): 0406002.
- [14] 陈吉欣, 陈少勇, 师勇, 等. 频率可调高性能光电振荡器研究[J]. 光学学报, 2013, 33(7): 0706016.
Chen J X, Chen S Y, Shi Y, et al. Research on optoelectronic oscillator with switchable frequency and high performance[J]. Acta Optica Sinica, 2013, 33(7): 0706016.
- [15] Wu B L, Wang M G, Dong Y E, et al. Magnetic field sensor based on a dual-frequency optoelectronic oscillator using cascaded magnetostrictive alloy-fiber Bragg grating-Fabry Perot and fiber Bragg grating-Fabry Perot filters[J]. Optics Express, 2018, 26(21): 27628-27638.
- [16] 韩晓晓, 徐恩明, 王斐, 等. 基于啁啾相移FBG的频率可调谐光电振荡器[J]. 光通信研究, 2016(6): 46-49.
Han X X, Xu E M, Wang F, et al. A frequency tunable optoelectronic oscillator based on a chirped phase-shifted FBG[J]. Study on Optical Communications, 2016(6): 46-49.
- [17] Wang Y P, Wang M, Xia W, et al. Optical fiber Bragg grating pressure sensor based on dual-frequency optoelectronic oscillator[J]. IEEE Photonics Technology Letters, 2017, 29(21): 1864-1867.
- [18] Yin B, Wang M G, Wu S H, et al. High sensitivity axial strain and temperature sensor based on dual-frequency optoelectronic oscillator using PMFBG Fabry-Perot filter[J]. Optics Express, 2017, 25(13): 14106-14113.
- [19] Tian X Z, Shi J Z, Wang Y P, et al. Sensitivity enhancement for fiber Bragg grating strain sensing based on optoelectronic oscillator with vernier effect[J]. IEEE Photonics Journal, 2021, 13(6): 5500106.
- [20] Feng D Q, Gao Y, Zhu T, et al. High-precision temperature-compensated magnetic field sensor based on optoelectronic oscillator[J]. Journal of Lightwave Technology, 2021, 39(8): 2559-2564.
- [21] Zhang B W, Kahrizi M. High-temperature resistance fiber Bragg grating temperature sensor fabrication[J]. IEEE Sensors Journal, 2007, 7(4): 586-591.
- [22] Kim J M, Kim C M, Choi S Y, et al. Enhanced strain measurement range of an FBG sensor embedded in seven-wire steel strands[J]. Sensors, 2017, 17(7): 1654.

Frequency Division Multiplexing Fiber Bragg Grating Sensing System Based on a Dual-Loop Optoelectronic Oscillator

Gao Lingge, Wang Yiping*, Tian Xiaozhong, Zhu Dan, Xiao Yunhao, Ge Jiawei, Chen Yingying

Jiangsu Key Lab on Opto-Electronic Technology, School of Computer and Electronic Information, Nanjing Normal University, Nanjing 210023, Jiangsu, China

Abstract

Objective Fiber Bragg grating (FBG) sensors are widely studied due to their unique advantages of light weight, small size, and sound stability in harsh environments. Most of the conventional demodulation methods for FBG sensing such as the filtering method, wavelength swept laser method, and tunable F-P filter method are performed in the optical domain, and they have the disadvantages of slow demodulation speed and low resolution. Therefore, it is important to develop new demodulation techniques with fast demodulation speed and high resolution. With the development of microwave photonics (MWP), the FBG sensing demodulation techniques based on an optoelectronic oscillator (OEO) have attracted extensive research interest. Compared with optical signals, microwave signals have relatively low frequencies and can be detected more rapidly and accurately. However, most of the current OEO-based FBG sensors are single-loop structures with large frequency fluctuations and a small free spectrum range (FSR) of the microwave signal output from the OEO, which results in a small measurement range and large measurement errors. Most importantly, only single parameter measurement can be realized. To this end, our paper proposes a frequency division multiplexing FBG sensing system based on a dual-loop OEO. We construct an optical dual-loop structure in the OEO loop and then perform frequency division multiplexing by a wavelength division multiplexer (WDM) and two electrical bandpass filters (EBPFs) with different center frequencies. This not only realizes the simultaneous sensing of strain and temperature but also significantly improves the measurement range and sensor stability.

Methods First, we employ two cascaded FBGs as the sensing heads for strain and temperature measurement respectively. Secondly, two optical loops 1 and 2 with great length differences are constructed to form a dual-loop structure to reduce the frequency fluctuation and increase the FSR of the output microwave signals. Then, the optical signal is divided into two paths by WDM and frequency division multiplexed by two EBPFs with different center frequencies to realize the simultaneous sensing. Finally, the wavelength-to-frequency mapping mechanism is adopted to demodulate the strain and temperature. In the experiment, we apply strain to FBG I and temperature to FBG II and gradually increase strain and temperature on FBG with a step of $45 \mu\epsilon$ and 6°C to obtain the sensing sensitivity. The

maximum frequency offset of the OEO output is recorded for ten minutes at different strains and temperatures to evaluate the stability of the OEO oscillation frequency. After that, the optical loop 2 is disconnected and the above steps are repeated to measure the sensing sensitivity and the maximum frequency offset of the frequency division multiplexing FBG sensing system based on a single-loop OEO. In addition, the measurement ranges of strain and temperature are estimated for single-loop OEO and dual-loop OEO structures respectively.

Results and Discussions By processing and analyzing the experimental data, an FSR of 5.01 MHz is obtained for the dual-loop OEO-based sensor (Fig. 2). The microwave oscillation frequency offset (Δf_{dual}) from the OEO output has a good linear relationship with the strain and temperature applied to the FBG, and the microwave oscillation frequency (f_{dual}) shifts to the high frequency region as strain and temperature increase [Figs. 3(a) and 3(c)]. The fitting results show a sensitivity of 0.100 kHz/ $\mu\epsilon$ for strain and 1.135 kHz/ $^{\circ}\text{C}$ for temperature [Figs. 3(b) and 3(d)]. The FSR of the single-loop OEO-based sensor is 177 kHz (Fig. 2), and the sensitivities of strain and temperature are 0.111 kHz/ $\mu\epsilon$ and 1.170 kHz/ $^{\circ}\text{C}$ respectively. Generally, the measurement range of the sensor is limited by the FSR of the OEO to avoid frequency ambiguity. Compared with the single-loop structures, the dual-loop structures substantially increase the measurement range of the sensor with little effect on the sensor sensitivity. In addition, the maximum frequency offset of the single-loop structure is 4.637 kHz and 4.420 kHz, corresponding to a measurement error of 42 $\mu\epsilon$ and 4 $^{\circ}\text{C}$ for the sensor [Fig. 4(a)]. The maximum frequency offset of the dual-loop structure is 0.035 kHz and 0.072 kHz respectively, with theoretical measurement errors as low as 0.35 $\mu\epsilon$ and 0.06 $^{\circ}\text{C}$ [Fig. 4(b)]. Therefore, the stability of the dual-loop OEO tracking signals is much higher than that of the single-loop OEO.

Conclusions We propose and experimentally demonstrate a frequency division multiplexing multifunction sensor based on a dual-loop OEO. By configuring two optical paths with different lengths in the dual-loop OEO structure, the FSR is expanded by about 28 times and the measurement range is improved. Compared with the measurement error of 42 $\mu\epsilon$ and 4 $^{\circ}\text{C}$ based on the single-loop OEO sensor, the theoretical measurement error of the dual-loop OEO is only 0.35 $\mu\epsilon$ and 0.06 $^{\circ}\text{C}$, which provides the sensor with high stability, large measurement range, and small measurement error. Two dual-loop OEO structures are formed by frequency division multiplexing through WDM and two EBPFs with different center frequencies, which allows strain and temperature to be sensed simultaneously. The sensing sensitivities of 0.100 kHz/ $\mu\epsilon$ and 1.135 kHz/ $^{\circ}\text{C}$ are obtained in the experiment. Additionally, if dense WDM and more EBPFs with different center frequencies are applied to our proposed sensors, more parameters can be measured in the form of a group network.

Key words sensor; optoelectronic oscillator; microwave photonics; frequency division multiplexing; fiber Bragg grating